

Robotic Hands with Intrinsic Tactile Sensing via 3D Printed Soft Pressure Sensors

Markellos Ntagios, Habib Nassar, Abhilash Pullanchiyodan, William Taube Navaraj, and Ravinder Dahiya*

Herein, the development of complex 3D intelligent structures such as robotic hands using innovative designs and multimaterial additive manufacturing technology is presented. The distal phalanges of the 3D printed hand presented herein have inherent soft capacitive touch or pressure sensors and embedded electronics. Materials such as thermoplastic polyurethane (TPU), silver paint, conductive polylactic acid composite, graphite ink, etc. are explored to develop five different variants of the sensors using a modified 3D printer, which is capable of extruding conductive ink, metal paste, and polymers. The best-performing 3D printed soft capacitive touch sensors, formed with silver paint and soft rubber (Ecoflex 00-30), are integrated on the distal phalanges of the 3D printed robotic hand. These sensors exhibit a stable response with sensitivity of 0.00348 kPa^{-1} for pressure $< 10 \text{ kPa}$ and 0.00134 kPa^{-1} for higher pressure. To demonstrate the practical applicability, the 3D printed hand with embedded soft capacitive touch sensors is used for interacting with everyday objects. The tightly integrated sensing elements within the 3D printed structures, as presented herein, can pave the way for a new generation of truly smart material systems that can possibly change their appearance and shape autonomously.

body or inside their rigid body to prevent devices from getting damaged during robotic operation.^[9] These robots, however, often fail to execute intricate tasks that are easily conducted by humans. They also cannot be used as the tools to understand the working of the human body as current arrangements do not allow synergistic working of sensors, actuation, and computation such as the arrangements that exist in humans.^[10] To realize their full potential, next-generation robots require soft sensors embedded in the body to provide distributed touch and haptic feedback.^[11] However, various touch sensors and eSkins developed for robots today, including those mimicking some human skin features such as fingerprints and increasing the tactile pixel (taxel) resolution,^[12–14] are developed on top of flexible and soft substrates to allow only their conformal placing on the outer surface of the body.^[4,6,15–17] This also comes with the


1. Introduction

Intrinsic or tightly integrated sensing, actuation, and computation into 3D structures could enable a new generation of truly smart and complex systems such as robots that have human-like dexterity, motor skills, and physical abilities that rely on feedback provided by the specialized receptors in the body.^[1–3] The field of robotics has strived to replicate these capabilities through flexible large-area eSkins,^[4–6] artificial muscles,^[7,8] computing devices, etc. that are either placed on the external surface of the robot's

challenge of wear and tear during frequent use.^[18] Here, we demonstrate a new approach to address the aforementioned issues by embedding the touch sensors in the distal phalanges of a 3D printed robotic/prosthetic hand that is robust, stable, and affordable.

The multimaterial 3D printing technique used here offers advances over current additive manufacturing (AM) strategies.^[19–21] Previous works have mainly focused on the printing of relatively thin structures, such as printed circuit boards (PCBs), or planar structures. Considering this, the advancement can be seen through the combination of extruded multimaterials to realize a tactile feedback mechanism for a robotic hand with the embedded electronics and sensors in 3D space. Moreover, the approach used here offers the ability to realize different types of structures without the need for expensive equipment, large-scale modifications, or expensive materials. AM is an attractive technique to realize embedded sensitive structures that cannot be manufactured using traditional micro/nanofabrication approaches, which usually involve multiple steps and are not cost effective.^[22–24] AM allows for easily customizable designs and on-site/on-demand production while reducing material waste, energy consumption, and prototyping time.^[25–28] Due to these benefits offered by 3D printing, new materials and processes are being developed to advance the technology beyond the typical 3D printed structures made from polymers.^[29,30] This is

M. Ntagios, H. Nassar, Dr. A. Pullanchiyodan, Dr. W. T. Navaraj, Prof. R. Dahiya
Bendable Electronics and Sensing Technologies (BEST) Group
School of Engineering
University of Glasgow
G12 8QQ Glasgow, UK
E-mail: Ravinder.Dahiya@glasgow.ac.uk

 The ORCID identification number(s) for the author(s) of this article can be found under <https://doi.org/10.1002/aisy.201900080>.

© 2019 The Authors. Published by WILEY-VCH Verlag GmbH & Co. KGaA, Weinheim. This is an open access article under the terms of the Creative Commons Attribution License, which permits use, distribution and reproduction in any medium, provided the original work is properly cited.

DOI: 10.1002/aisy.201900080

particularly important for complex shapes such as robotic hands which require distributed touch sensors embedded in the structure. To this end, there is need to advance the AM technique toward simultaneous multimaterial printing, i.e., printing of conductive or photosensitive materials and polymers to be incorporated in the 3D printing process. In this regard, recent works such as patterning of liquid metals by direct writing and filling predefined microchannels to develop conductors,^[31–39] multilayered circuit boards, and antennas, etc. for applications in the fields of biomedical, aerospace, and electronic engineering are worth mentioning.^[40–49] However, printed conductors in a 2D plane shown in the previous works are insufficient for a robot's body as the sensors need to be embedded at different depths. This can be achieved by innovative hand designs with intrinsic sensors along with 3D printing of multimaterials.^[50–53]

To illustrate this capability, here we demonstrate the 3D printed soft capacitive sensor, with a capacitance-to-digital converter chip on a PCB, fully embedded into the 3D printed robot hand to deliver pressure-sensing and signal-processing operations. First, a five-finger 3D printed hand is presented with embedded actuators for the movement of the fingers. Then, the multimaterial 3D printing approach is demonstrated to obtain soft capacitive pressure-sensing phalanges. As exemplified in **Figure 1**, conductive and dielectric layers of capacitive

sensors and the conductive tracks are printed within the 3D printed fingers using a modified 3D printer. The 3D printer used is a desktop fused deposition modeling (FDM) printer with an added custom-made second printing nozzle for paste/ink printing (Figure S1, Supporting Information). The paste extruder is not placed directly on the x-carriage of the printer to prevent the added weight causing misalignment of the nozzles and the print bed and reduce vibrations during printing which can reduce the print quality. The added extruder uses a syringe and a Bowden tube to connect to the printer and its stepper motor is connected to the printer's electronics board. The necessary firmware adjustments to incorporate the second nozzle parameters with a different stepper feed rate were implemented. The embedded capacitive pressure-sensing phalanges were designed and compared as five types were fabricated using different flexible dielectric and conductive materials. A two-part rubber and commercially available flexible thermoplastic polyurethane (TPU) were used as the dielectric, and a silver paste, commercially available conductive polylactic acid (PLA) composite, and an in-house made graphite ink were used as the electrodes for different samples of the capacitive sensor. The best-performing combination of dielectric and conductive materials (i.e., silver paint and soft rubber (Ecoflex 00-30)) for the soft capacitive sensor was used in the robotic/prosthetic hand for tactile feedback

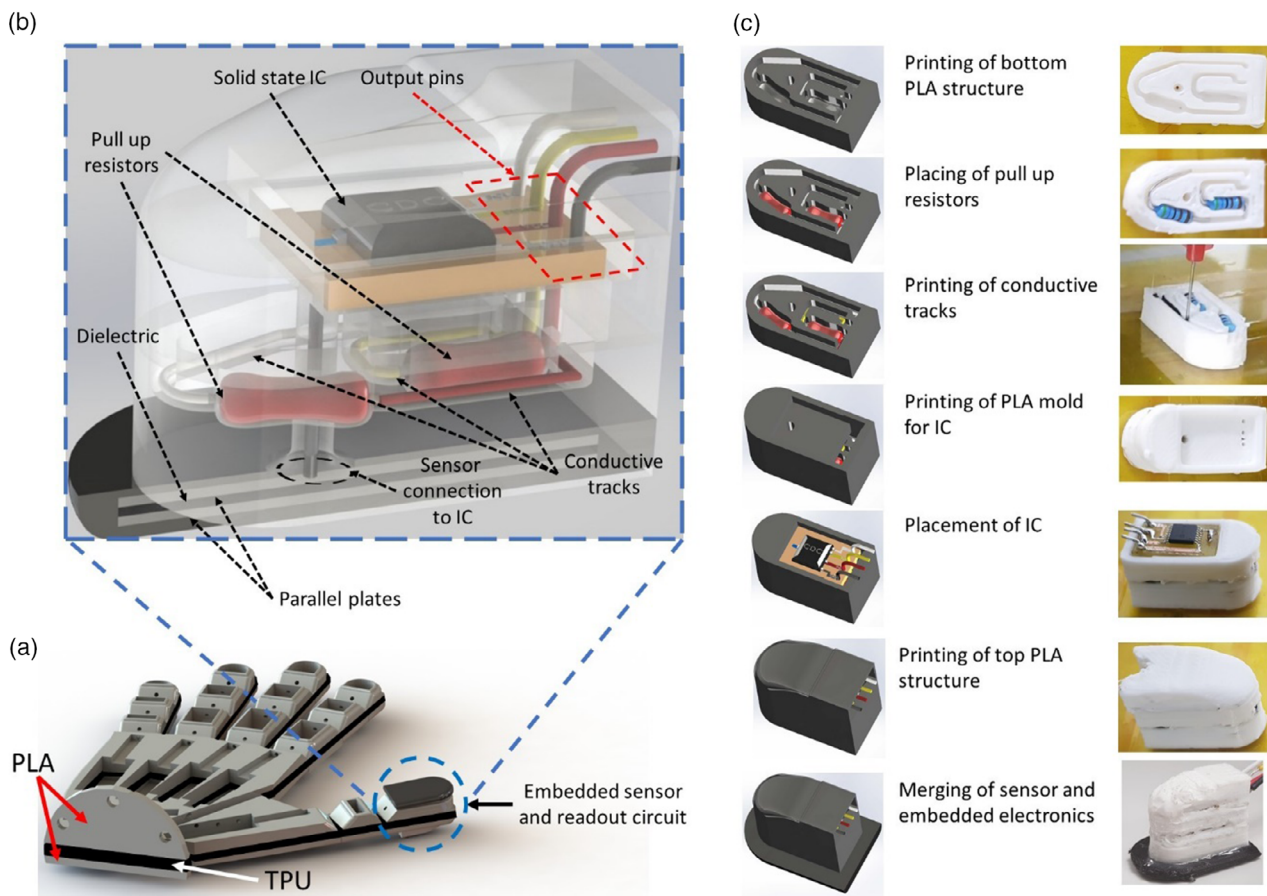


Figure 1. The 3D printed hand with intrinsic tactile sensing. a) CAD design of the hand with the smart sensing phalanx having a soft capacitive touch sensor and an embedded readout circuit. b) CAD design of the interior structure of the phalanx. c) Fabrication steps for the 3D printed phalanx.

(Figure 1a). The sensors can be tunably printed within both stretchable and rigid substrates and can provide standalone functionalities. The printing of conductive layers also provides an opportunity to integrate the readily available silicon integrated circuit (ICs) (Figure 1b) to realize a sensorized robotic body with distributed sensing and computing. This has been demonstrated here by the embedding of an electronic circuit board within the distal phalanx of the 3D printed hand (Figure 1c). Integration of silicon IC chips will enable advanced circuit functionalities (e.g., distributed computing) that would not have been achieved otherwise by 3D printed liquid-state components alone. Finally, we demonstrate the application of an innovative 3D printing process to deliver sensorized robotic/prosthetic hands that are affordable and at the same time offer more functionalities than conventional rigid-body robotic hands.

2. Design of Hand and Embedded Pressure Sensing Phalanx

The 3D printed hand was designed to utilize the capabilities of multimaterial 3D printing offered by state-of-the-art 3D printers with a layered architecture to ensure easy printability without the requirement of any support structure. The palm area of the hand has six slots for six PQ12-63-6-R microlinear actuators (two actuators for the thumb and four for the rest of the fingers). The hand was fabricated using three different 3D printing materials (Figure 1). The hand is segmented into three sections: bottom, middle, and top (Figure 1a) and was printed in a layered fashion.

The first layer is PLA (of 4 mm thickness) followed by a second layer involving acrylonitrile butadiene styrene (ABS) (of 1 mm thickness). The adhesion between ABS and TPU is much higher than that between TPU and PLA. Hence, the second thin layer of ABS was used followed by TPU which forms the third layer. This is followed by a fourth layer of ABS followed by a final PLA layer. The multimaterial printing was possible as the printer used for hand has the capability to print three materials from its three nozzles. The layered arrangement utilizes the rigidity of PLA/ABS as a skeletal support structure, whereas the elasticity of TPU is used to achieve flexion of the finger joints. The hand was printed without any use of support material. In Table S1, Supporting Information, we have summarized the adhesion relations between all the materials used in this study. The fingers are actuated via a tendon mechanism. The tendons were connected to the distal phalanges and were pulled through slots in the hand via microlinear actuators to achieve desired flexion. During extension, the linear actuator is released, and the joints get back to the normal state as the TPU reverses back from its elastic deformed bent state. The fingers are designed to have TPU only at the joints. The absence of PLA at the joints, and owing to TPU's elasticity, the fingers can bend easily with a single actuator used for each finger. Furthermore, the phalanges have been designed with gaps to embed the electronics related to intrinsic touch sensors.

The full design of the intrinsic touch sensor is shown in Figure 2a. The simple design makes it easy to fabricate the embedded capacitive pressure-sensing phalanx using the different combinations of materials. In some way, the architecture of the phalanx imitates the human distal phalanx which consists of

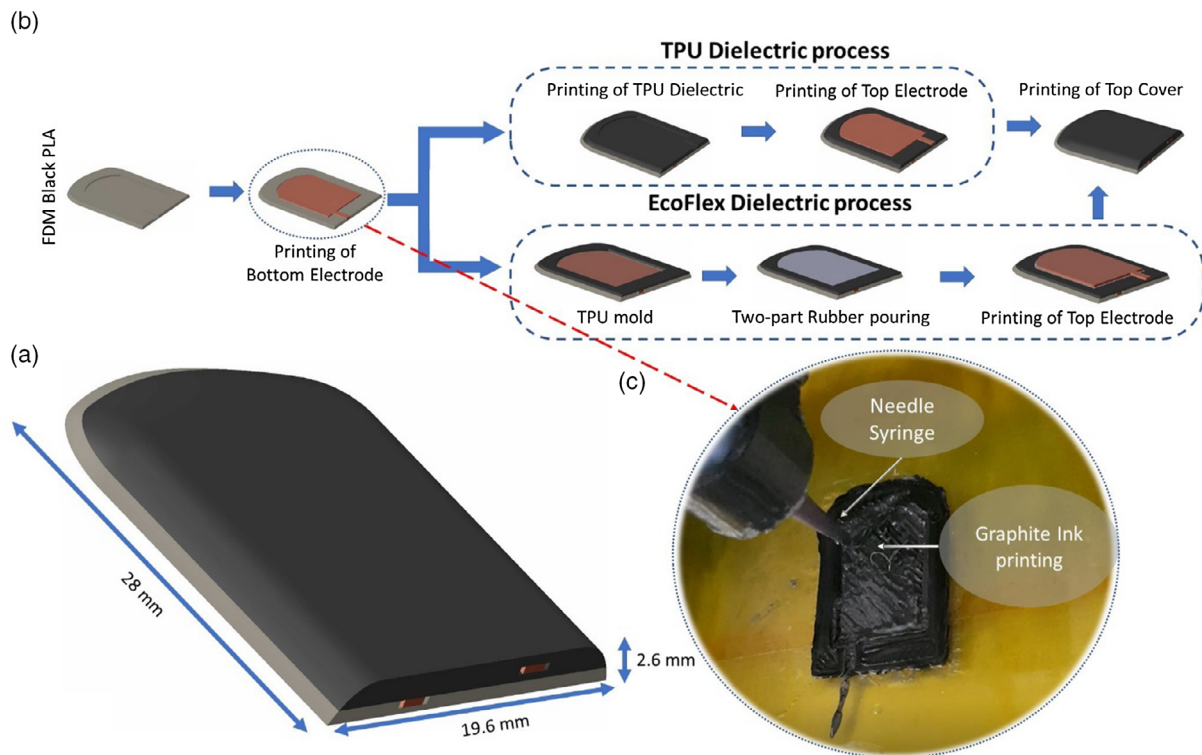


Figure 2. Capacitive pressure-sensing part of the phalanx showing a) the complete structure of the phalanx, b) the fabrication procedure of the TPU and two-part rubber dielectric, and c) the graphite ink printing using the modified desktop 3D printer capable of cold extrusion.

the bone with soft tissue and skin around. The design resembles this pattern with a rigid base made from black PLA, the conductive and the dielectric elements mimicking the soft tissue, and the top layer of the TPU 3D printing filament (Young's modulus of 12 MPa) resembling the elastic properties of the human skin which has a Young's modulus of 5–20 MPa.^[54] The embedded capacitive pressure-sensing phalanx has two computer-aided design (CAD) model variations to compensate for the different fabrication techniques required for the two types of dielectric materials explored here. Figure 2b shows the fabrication processes of the two variations of the phalanx designs with different dielectric materials.

The embedded capacitive pressure sensor is 19.6 mm wide, 2.6 mm thick, and 28 mm high. The phalanx structure has five parts: base structure, bottom electrode, dielectric, top electrode, and top polymer layer. A mould for the bottom electrode is designed on top of the base structure and filled with the conductive material for the formation of the capacitive sensor. Each electrode is 14 mm wide, 0.5 mm thick, and 19.2 mm high. The distance between the bottom electrode and the surrounding walls of the base structure is 0.3 mm. Similar to the bottom electrode, the top electrode has a separation distance of 0.3 mm from the surrounding walls. This offset/gap prevents the 3D printer nozzles from colliding into the existing fabricated structure during printing. There are two access points in the 3D printed phalanx, one for each electrode of the capacitive-sensing element. The overlapping surface area of the two parallel plates is 250 mm² and the dielectric thickness between them is 0.5 mm.

With regard to the embedded electronics in the phalange, the scheme to read out the capacitive sensor is shown in Figure S2, Supporting Information. The fabrication of the phalange with embedded electronics followed a few steps. First, the bottom layer was printed with PLA and then the channel for the embedded pull-up resistors as well as the conductive channels was realized using the in-house graphite ink. The conductive ink in the channels was printed using the Discov3ry paste extruder system. A second PLA layer was then printed on top of the resistors and channels to fully embed them, while incorporating vertical, out-of-plane channels to connect the first layer to the top one in a 3D fashion. This is where the 3D circuitry is implemented. Finally, the surface mount device (SMD) capacitance-to-digital convertor chip (soldered to a very small breakout PCB) was placed in the structure (Figure 1) and connected to the 3D channels to form the thumb phalange with tightly packed electronics inside. Wires were then taken out for external communication of the sensed pressure data. The thumb capacitive pressure sensor was fabricated as mentioned previously but with an added channel to connect with the other electronics.

3. Experimental Section

3.1. Materials

3.1.1. Conductive Materials

Three conductive materials were used for the formation of the parallel capacitance plates: a commercially available silver conductive paint (RS Components 186-3600, having resistivity

(ρ) = 0.001 Ω cm), a commercially available conductive PLA (proto-pasta CDP11705, ρ = 15 Ω cm), and an in-house formulated graphite-based ink (ρ = 2.6 Ω cm). The major reason for the use of these conductive materials was their printability using our customized 3D printer. However, the adhesion of the conductive materials with the substrate was a limiting factor.

3.1.2. Dielectric Materials

Two dielectric materials were used to form the capacitive sensor. The first dielectric used was a two-part silicone rubber (Ecoflex 00-30, Smooth-On, Inc) that has high elasticity with a Young's modulus of 27.24 kPa and a dielectric constant of 2.8.^[55,56] This material is capable of withstanding high temperatures, which is a requirement due to the FDM process used in the fabrication of the sensor. The second dielectric used was a flexible TPU (NinjaFlex 85A, NinjaTek) 3D printing filament, with a tensile modulus of 12 MPa and a dielectric constant of 3.^[57] These materials are used to investigate the effect of the packaging on the response of the sensor in contrast to the elastic modulus of the dielectric.

Three devices for each type were fabricated from the combinations of these materials. In addition, a sixth type of the device was fabricated with TPU as the dielectric and conductive PLA forming the parallel plates of the capacitor. However, the higher temperature required for the extrusion of TPU, compared with conductive PLA, resulted in the mixing of the dielectric and conductive materials while printing and prevented the formation of the transducer.

3.2. Methods

3.2.1. Ink Formulation

The graphite ink, used in this study, was realized for the formation of the parallel plates of one of the 3D printed capacitive sensors. The graphite ink was formulated in an organic solvent-based system. Initially, 0.5 g of Triton X-100 (Sigma Aldrich) and 0.35 g of polyethylene glycol (Sigma Aldrich) were dissolved in 9.0 mL of terpineol (Sigma Aldrich) solvent by magnetic stirring for 30 min. After that, the binder ethyl cellulose (0.15 g, Sigma Aldrich) was added and the mixture was stirred for 1 h. Finally, 4.0 g of graphite powder (Sigma Aldrich) was added and the mixture was continuously stirred for 6 more hours to obtain a well-homogenized stable ink. The electrical resistivity of the developed ink was measured using a four-probe method on the printed pattern.

3.2.2. Device Fabrication

To fabricate the presented sensing devices, an open-source desktop 3D printer (RepRap Ormerod 2) was customized to be able to extrude conductive pastes (Figure 2c). In all variations, the base structure was fabricated using the traditional FDM method. The bottom and top plates of the capacitive sensor were fabricated with different techniques, depending on the material used. For example, the silver adhesive paint was applied with a brush, the conductive PLA was deposited using the traditional FDM

process, and the graphite ink was deposited using the paste extrusion setup added to the 3D printer. The flexible elastomer used as a dielectric was deposited from the original extruder of the modified 3D printer using FDM. In contrast, the two-part rubber was prepared separately with the parts mixed in a 1:1 volume ratio. The rubber was poured on top of the bottom electrode and the excess material was removed with a flat tool by slightly pressing the top of the structure. The adhesion of both the two-part rubber and the graphite ink with the other printable materials was found to be poor and the FDM deposition of materials on top of them was not possible. To overcome this problem, a thin layer of Kapton film was placed on the top of two materials to enable FDM. After the deposition of the top electrode, the full encapsulation of the sensing element was done via FDM printing of the top polymer part.

3.2.3. Two-Part Rubber Preparation

The two-part rubber was mixed together in a 1:1 volume ratio for 3 min and kept under vacuum for 1 min to remove air trapped in the mixture. After that, it was poured on top of the device. The device was placed on the build plate of the 3D printer, which was set at 60 °C, and a hot air gun (set at 100 °C) was directed on top of the device for 1 h with minimal flow to accelerate the curing process of the EcoFlex.

3.2.4. Printing of Black PLA/Conductive PLA (RS PRO 1.75 mm Black PLA 3D Printer Filament -Proto-Pasta CDP11705)

The print settings of black PLA and conductive PLA were identical. The layer height was set to 0.1 mm with 100% infill and printing speed of 60 mm s⁻¹. The printing temperature was set to 200 °C with the heated bed set at 60 °C.

3.2.5. Printing of TPU

Before printing, the TPU filament was placed in an incubator at 50 °C for 30 min to remove moisture from the filament, to increase the printing quality of the material. After that, the filament was mounted on the 3D printer. The layer height was set to 0.1 mm with 100% infill, but the printing speed

was reduced to 10 mm s⁻¹ as TPU, in general, requires low printing speeds to extrude and print reliably.

3.2.6. Printing of Graphite Ink

After stirring, the graphite ink was used to fill the syringe connected to the DISCOV3RY 2.0 system (Structur3D Printing) for paste extrusion. The internal diameter of the nozzle used to extrude the paste was 0.51 mm with the printing layer height set to 0.25 mm and the print speed set to 3 mm s⁻¹. After the printing process, the print bed was heated to 60 °C and a hot air gun was used at 100 °C to dry the composite for 2 h. After the drying process, a Kapton polyimide sheet with a piece of chemical-resistant tape (RS Components) was cut into the shape of the phalanx and placed on top of graphite to enable further FDM procedures.

4. Results and Discussion

4.1. Results

For each type of sensor, a set of three devices was fabricated and characterized. Once the sensors were fabricated, the characterization process followed. The devices were placed on a load cell (Figure S3, Supporting Information) and force was applied on the top via an actuator controlled by a LabVIEW program. The capacitance was measured using a resistance, inductance, capacitance meter. The five different fabricated embedded capacitive pressure-sensing phalanges, namely Ecoflex-silver (Eco-Ag), Ecoflex-graphite (Eco-Grp), Ecoflex-conductive PLA (Eco-PLA), thermoplastic polyurethane-silver (TPU-Ag), and thermoplastic polyurethane-graphite (TPU-Grp), are shown in **Figure 3a–e**. All five devices were tested for their sensing capabilities and **Table 1** summarizes the average sensitivity and linearity, in the entire tested range, of all the types and the amount of drift for all sensors. **Figure 4** shows the average relative change of capacitance of each type with respect to increasing pressure from 0 Pa to 50 kPa. It is clear from the figure that all types show an increase in capacitance with an increase in applied pressure. However, the rate of change in capacitance in each type is not

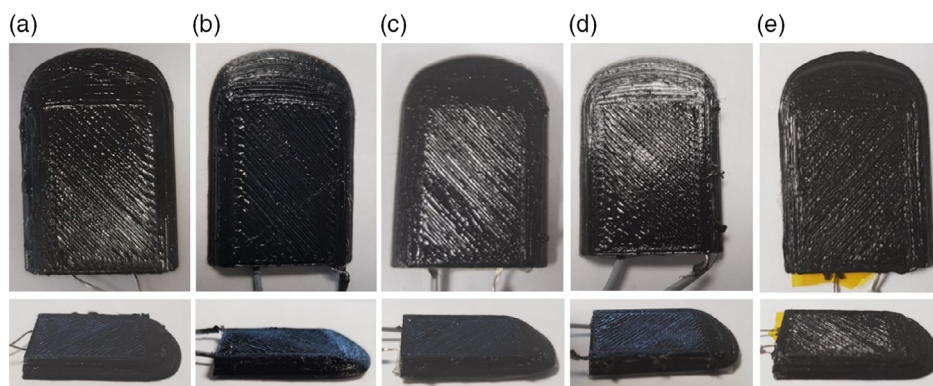


Figure 3. 3D printed devices with sensor structures comprising a) silver paint with two-part rubber dielectric, b) silver paint with TPU dielectric, c) graphite ink with two-part rubber dielectric, d) graphite ink with TPU dielectric, and e) conductive PLA with two-part rubber dielectric.

Table 1. Specifications of the five types of sensors.

1	Eco-Ag			Eco-graphite			Eco-PLA			TPU-Ag			TPU-graphite		
Sensitivity [kPa^{-1}]	0.002115			0.001214			0.00218			0.000651			0.003		
Linearity	0.80			0.33			0.99			0.58			0.93		
Drift ($\times 10^{-4} \text{min}^{-1}$)	S1	S2	S3	S1	S2	S3	S1	S2	S3	S1	S2	S3	S1	S2	S3
	5.6	1.9	0	-10	7	6	8	18	4	1.6	2.1	-0.6	3.6	21	2.1

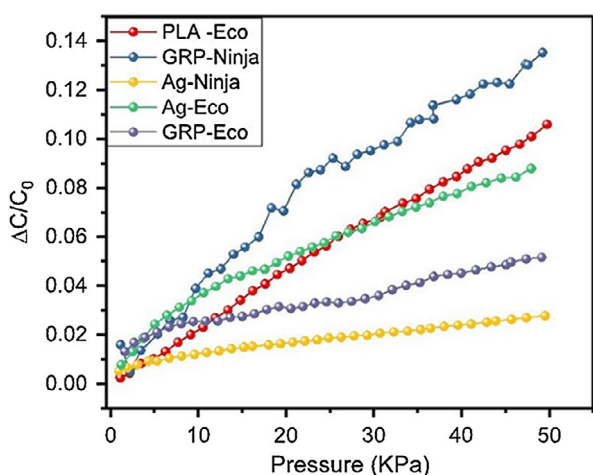


Figure 4. The average change in the relative capacitance of the five printed sensing devices with increase in pressure.

the same. Figure S4, Supporting Information, shows all the characterizing results of all the devices besides the Eco-Ag.

All devices were tested under a constant pressure of 20 kPa for 8 min. The devices were also tested for hysteresis from 0 kPa to 50 kPa. Finally, the devices were tested for their dynamic cycle response with increasing pressure (0–50 kPa).

Among the tested types, the TPU-Grp devices, on average, showed the highest sensitivity (0.00309 kPa^{-1}) in the tested pressure range from 0 Pa to 50 kPa. The linearity was found to be 0.932. The Eco-PLA devices were found to have an average sensitivity of 0.00218 kPa^{-1} . The linearity of the devices is 0.99 in the entire tested range, with significant deviation in sensitivity among them. Another detriment of this type is that all devices showed the highest amount of hysteresis compared with all devices of the other types, specifically in the range of 10–30 kPa.

In contrast, the Eco-Grp showed irreproducible results. One of the devices showed instability in all characterization tests. Two of the devices showed an increase in capacitance over time under a constant load, while the third one showed an unstable response with a general trend of decreasing capacitance. The average sensitivity of all devices was found to be 0.00121 kPa^{-1} . There are two linear regions, one from 0 to 14 kPa with sensitivity of 0.00256 kPa^{-1} and a second from 14 to 50 kPa with sensitivity of $0.000721 \text{ kPa}^{-1}$. From hysteresis testing, all devices show hysteresis but not in the same pressure region. The first device showed hysteresis in the entire tested range with the second showing hysteresis in the 25–35 kPa range and the last showing

hysteresis in the 10–25 kPa range. Due to the aforementioned issues, this type of sensor was found to be unreliable for the current application.

The devices formed by TPU and silver show minor drift. The response of each device varies significantly and the average sensitivity for the entire range was found to be 0.00065 kPa^{-1} . Two devices exhibit hysteresis in two different pressure ranges: the first in the range of 25–35 kPa with the second in range of 10–25 kPa. This type of device showed the lowest sensitivity compared with the others.

The Eco-Ag devices exhibit superior performance among the rest of the devices, capable of reliably sensing pressures as low as 1 kPa. All three devices showed high stability and reproducibility in their response. All devices showed insignificant drift for over 8 min of constant pressure. High sensitivity was observed up to 10 kPa at 0.00374 kPa^{-1} , whereas for pressures above 10 kPa, the sensitivity of the devices dropped to 0.00134 kPa^{-1} with a linearity of 0.996. All three devices have similar responses to each other with minor deviations. Repeatability and reproducibility of the sensors were major factors for choosing this type to integrate with the embedded readout circuit. Figure 5a shows one of the three Eco-Ag devices' relative change in capacitance over time with an increase of pressure every second cycle (from 0 Pa to 50 kPa) for over 100 loading and unloading cycles. It was noted that all the devices showed similar response trends, as well as excellent stability and repeatability in the tested range. Similar testing was conducted for the rest of the devices. Figure S5, Supporting Information, shows the cycling testing for one sensor of each type.

Figure 5b shows the relative change of capacitance response of one of the Eco-Ag devices under loading and unloading with respect to time. This test can be segmented into three phases: pre-load, load, and unload phase. The sensor in the pre-load condition was subjected to a static load of 6.6 kPa. Then, pressure was increased to 18 kPa for a small period of time, indicating the load phase. The sensor's response time to a sudden change in pressure is in the order of a hundred milliseconds. Then, the pressure was reduced back to the previous level during the final unload phase. The device's response is, again, in the range of a few hundred milliseconds with minor deviation before and after the load phase. The devices were tested under a constant pressure and all of them showed minor deviation over time (Figure 5c). Figure 5d,e shows the relative change of capacitance over an increase in pressure and hysteresis of each of the three fabricated devices of this variation. All three sensors have similar behavior with good reproducibility. From the above, we conclude that the two-part rubber with the silver adhesive paint had the superior performance in comparison with the rest of the fabricated devices.

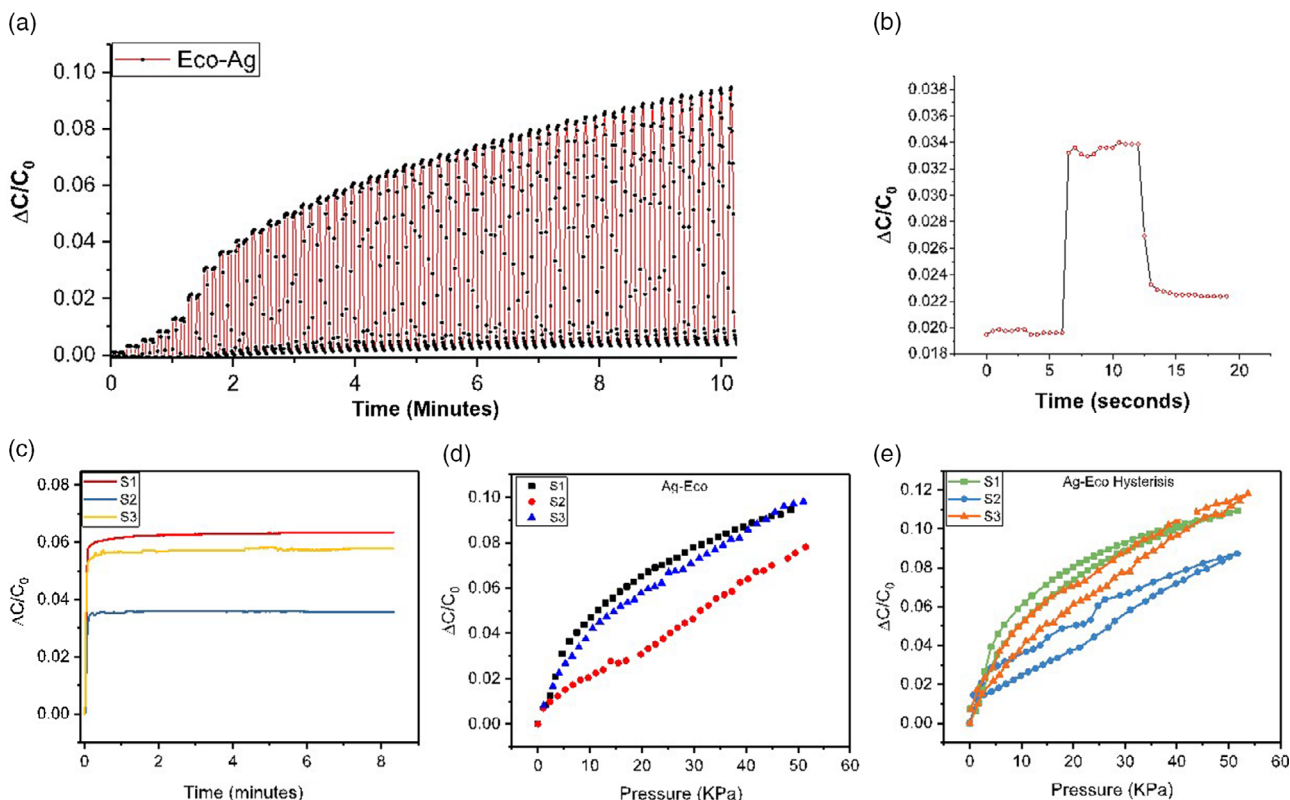


Figure 5. a) Dynamic response of one of the Eco-Ag sensing devices over time with increasing pressure. b) Relative change in capacitance of the Eco-Ag sensing device with respect to time during one of the loading–unloading cycles. c) Response of all three sensors under constant load. d) Relative change in capacitance with increasing pressure. e) Hysteresis curve of the tested devices.

The TPU-Ag devices showed the lowest sensitivity on an average. This was the main factor for discarding this type as a tactile feedback sensor. This can be attributed to the elastic modulus of the TPU as its elastic modulus is almost two orders of magnitude higher than that of EcoFlex.

The graphite ink devices when combined with the TPU dielectric are less reproducible, despite their higher average sensitivity. The large deviation and unusual behavior in sensitivity of each graphite-based device compared with the silver-based devices may be due to the formation of microcracks in the graphite-printed film, which tend to propagate with application of higher amounts of pressure. This can be observed from hysteresis and cyclic tests for both graphite-based devices (Figure S4, S5, Supporting Information). The two devices with low sensitivity made from TPU and the graphite ink have an average sensitivity of 0.00145 kPa^{-1} —a comparable sensitivity to the TPU-Ag devices. Nonetheless, the graphite ink could be used to develop connections between the sensor and the readout circuit, where chances of deformation or cracking are low. This will be a low-cost interconnect which can be used in an automated 3D printing process.

Similarly, the phalanges fabricated from the graphite ink and the two-part rubber (Eco-Grp) have low sensitivity ($0.001214 \text{ kPa}^{-1}$). As mentioned earlier, the graphite ink starts to crack even under small amounts of pressure. In one of the devices, this effect can be seen clearly in the hysteresis of the

device. This effect can be seen in both variations of the graphite-based devices. As a result, the sensors containing the ink were discarded for the use in the robotic/prosthetic hands as tactile sensors.

Eco-PLA variation shows good response in terms of sensitivity with an average of 0.00218 kPa^{-1} and a linear response in the entire tested range. The devices showed good stability, but they also showed the highest hysteresis.

The superiority of the Eco-Ag devices over the rest of the devices is due to the material properties of the silver adhesive and the two-part rubber. The surface roughness of the silver was compensated for by the capability of the two-part rubber to surround the adhesive and establish a strong bond between them. Moreover, silver did not show a paste-like behavior, such as graphite ink, after curing. The silver adhesive paint, even as a fragile material after curing, showed exceptional robustness in the packaged phalange.

This embedded capacitive pressure-sensing phalanx was integrated on the 3D printed robotic hand described earlier to provide the force or pressure feedback.

5. Application

To demonstrate the potential of the presented approach for robotic hands with intrinsic tactile sensing, five modular sensors

based on the Eco-Ag variation were printed and mounted on the distal phalanges of a 3D printed prosthetic hand. A custom PCB was designed to read out the data from the sensors and transmit the data to a computer via a universal serial bus (USB) cable (Figure S6, Supporting Information). A LabVIEW program was designed for the representation of the data captured from the integrated circuits on the PCB. **Figure 6a–e** shows the 3D printed hand with integrated soft capacitive sensors. On the right side of the figures, the graphs represent the real-time response of the sensors on the five distal phalanges. As pressure is applied on them, the capacitance increases, and this change can be observed from the graph. (Supporting Video 1, Supporting Information).

The 3D printed hand with intrinsic touch sensing was also tested for interacting with objects and actuation, capturing the

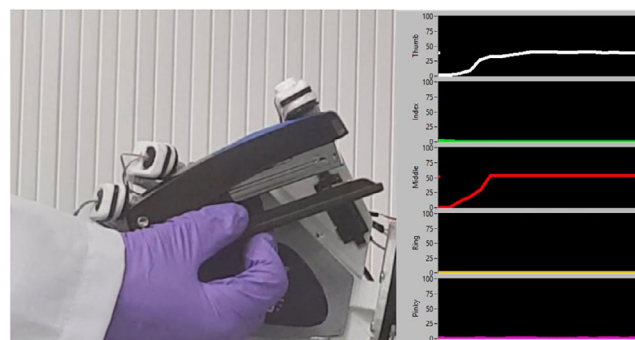


Figure 7. 3D printed hand with intrinsic sensing responding to touch while actuating. The hand is integrated with a UR5 robotic arm.

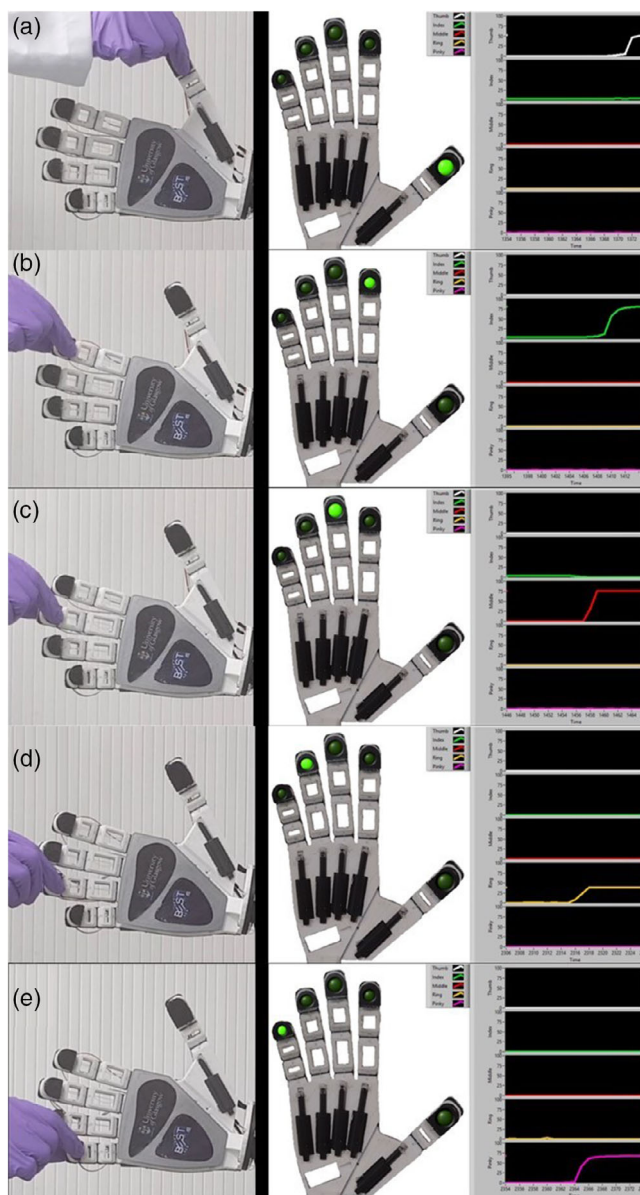


Figure 6. Modular-embedded capacitive pressure-sensing distal phalanges (a–e) on a robotic hand responding to pressure stimuli shown via LabVIEW.

response by the LabVIEW graphical user interface (Supporting Video 2, Supporting Information). We noted that the hand can interact with common objects (**Figure 7**).

6. Conclusion

The 3D printed hand with embedded soft capacitance pressure sensing presented in this article is an interesting approach for obtaining complex smart structures with intrinsic sensing, actuation, and computing. The sensors obtained are quite sensitive and can sense pressures as low as 1 kPa. The tightly integrated sensing within the 3D printed structures could pave the way for a new generation of truly smart material systems that can change their appearance and shape autonomously. The simplicity of the fabrication process presented here introduces a cost-effective alternative fabrication method for tactile sensing systems that otherwise require complex, expensive, and specialized equipment. In this regard, compared with the state-of-the-art robotic or prosthetic hands, the presented approach could lead to robust and affordable hands with more functionalities. Furthermore, the multimaterial 3D printing methodology offers efficient use of 3D space through embedded components, and in this regard, this work presents advances in AM technology.

Supporting Information

Supporting Information is available from the Wiley Online Library or from the author.

Acknowledgements

This work was supported in part by the Engineering and Physical Sciences Research Council (EPSRC) through National Productivity Investment Fund (EP/R512266/1) and Shadow Robot Company LTD, UK.

Conflict of Interest

The authors declare no conflict of interest.

Keywords

additive manufacturing, capacitive sensors, intrinsic sensing, material integrated sensing, multimaterial 3D printing, robotic hands, soft robotics

Received: July 15, 2019

Revised: September 3, 2019

Published online:

-
- [1] R. S. Dahiya, in *Proc. IEEE* **2019**, Vol. 107, p. 247.
- [2] D. Rus, M. T. Tolley, *Nature* **2015**, 521, 467.
- [3] M. A. McEvoy, N. Correll, *Science* **2015**, 347, 1261689.
- [4] R. S. Dahiya, W. T. Navaraj, S. Khan, E. O. Polat, *Inf. Disp.* **2015**, 31, 6.
- [5] C. G. Núñez, W. T. Navaraj, E. O. Polat, R. S. Dahiya, *Adv. Funct. Mater.* **2017**, 27, 1606287.
- [6] C. García Núñez, L. Manjakkal, R. S. Dahiya, *Flexible Electron.* **2019**, 3, 1.
- [7] E. T. Roche, R. Wohlfarth, J. T. B. Overvelde, N. V. Vasilyev, F. A. Pigula, D. J. Mooney, K. Bertoldi, C. J. Walsh, *Adv. Mater.* **2014**, 26, 1200.
- [8] M. Taghavi, T. Helps, J. Rossiter, *Sci. Robot.* **2018**, 3, eaau9795.
- [9] W. Taube Navaraj, C. García Núñez, D. Shakthivel, V. Vinciguerra, F. Labeau, D. H. Gregory, R. Dahiya, *Front. Neurosci.* **2017**, 11, 501.
- [10] R. Dahiya, M. Valle, *Robotic Tactile Sensing: Technologies and System*, Springer Science & Business Media, Dordrecht **2013**.
- [11] R. S. Dahiya, P. Mittendorfer, M. Valle, G. Cheng, V. J. Lumelsky, *IEEE Sens. J.* **2013**, 13, 4121.
- [12] C. Wang, D. Hwang, Z. Yu, K. Takei, J. Park, T. Chen, B. Ma, A. Javey, *Nat. Mater.* **2013**, 12, 899.
- [13] M. L. Hammock, A. Chortos, B. C. K. Tee, J. B. H. Tok, Z. Bao, *Adv. Mater.* **2013**, 25, 5997.
- [14] W. Navaraj, R. Dahiya, *Adv. Intell. Syst.* **2019**, 1, 1900051.
- [15] R. S. Dahiya, G. Metta, M. Valle, G. Sandini, *IEEE Trans. Robot.* **2010**, 26, 1.
- [16] N. Yogeswaran, W. Dang, W. T. Navaraj, D. Shakthivel, S. Khan, E. O. Polat, S. Gupta, H. Heidari, M. Kaboli, L. Lorenzelli, G. Cheng, R. S. Dahiya, *Adv. Robot.* **2015**, 29, 1359.
- [17] H. Yousef, M. Boukallel, K. Althoefer, *Sens. Actuators A Phys.* **2011**, 167, 171.
- [18] M. Ntagios, W. T. Navaraj, R. S. Dahiya, presented at IEEE SENSORS, New Delhi, India, October 2018.
- [19] X. Wang, M. Jiang, Z. Zhou, J. Gou, D. Hui, *Composites B* **2017**, 110, 442.
- [20] K. V. Wong, A. Hernandez, *ISRN Mech. Eng.* **2012**, 2012, 1.
- [21] T. D. Ngo, A. Kashani, G. Imbalzano, K. T. Nguyen, D. Hui, *Compos. B Eng.* **2018**, 143, 172.
- [22] E. MacDonald, R. Wicker, *Science* **2016**, 353, aaf2093.
- [23] B. Berman, *Bus. Horiz.* **2012**, 55, 155.
- [24] Y. Ni, R. Ji, K. Long, T. Bu, K. Chen, S. Zhuang, *Appl. Spectrosc. Rev.* **2017**, 52, 623.
- [25] P. F. Flowers, C. Reyes, S. Ye, M. J. Kim, B. J. Wiley, *Addit. Manuf.* **2017**, 18, 156.
- [26] J. W. Stansbury, M. J. Idacavage, *Dent. Mater.* **2016**, 32, 54.
- [27] R. Bogue, *Assemb. Autom.* **2013**, 33, 307.
- [28] B. Mueller, *Assemb. Autom.* **2012**, 32.
- [29] G. Postiglione, G. Natale, G. Griffini, M. Levi, S. Turri, *Compos. A* **2015**, 76, 110.
- [30] R. L. Truby, J. A. Lewis, *Nature* **2016**, 540, 371.
- [31] J. W. Boley, E. L. White, G. T. C. Chiu, R. K. Kramer, *Adv. Funct. Mater.* **2014**, 24, 3501.
- [32] D. Periard, E. Malone, H. Lipson, presented at 18th Solid Freeform Fabrication Symposium, Austin, TX, August 2007.
- [33] J. A. Lewis, *Adv. Funct. Mater.* **2006**, 16, 2193.
- [34] S. Y. Wu, C. Yang, W. Hsu, L. Lin, *Microsyst. Nanoeng.* **2015**, 1, 15013.
- [35] Y. L. Park, C. Majidi, R. Kramer, P. Bérard, R. J. Wood, *J. Micromech. Microeng.* **2010**, 20, 125029.
- [36] M. D. Dickey, R. C. Chiechi, R. J. Larsen, E. A. Weiss, D. A. Weitz, G. M. Whitesides, *Adv. Funct. Mater.* **2008**, 18, 1097.
- [37] H. Nassar, M. Ntagios, W. T. Navaraj, R. S. Dahiya, presented at IEEE SENSORS, New Delhi, India, October 2018.
- [38] J. Park, S. Wang, M. Li, C. Ahn, J. K. Hyun, D. S. Kim, D. K. Kim, J. A. Rogers, Y. Huang, S. Jeon, *Nat. Commun.* **2012**, 3, 916.
- [39] R. K. Kramer, C. Majidi, R. J. Wood, *Adv. Funct. Mater.* **2013**, 23, 5292.
- [40] G. J. Hayes, S. C. Desai, Y. Liu, P. Annamaa, G. Lazzi, M. D. Dickey, *Microwave Opt. Technol. Lett.* **2014**, 56, 1459.
- [41] V. Palazzi, W. Su, R. Bahr, S. Bittolo-Bon, F. Alimenti, P. Mezzanotte, L. Valentini, M. M. Tentzeris, L. Roselli, *IEEE Trans. Compon. Packag. Manuf. Technol.* **2019**, 9, 1434.
- [42] M. A. C. Angeli, F. Nikbakhtnasrabadi, P. Vena, R. S. Dahiya, presented at IEEE FLEPS, Glasgow, UK, July 2019.
- [43] H. Ota, S. Emaminejad, Y. Gao, A. Zhao, E. Wu, S. Challa, K. Chen, H. M. Fahad, A. K. Jha, D. Kiriya, *Adv. Mater. Technol.* **2016**, 1, 1600013.
- [44] M. Ahmadloo, P. Mousavi, presented at Microwave Symposium Digest (IMS), 2013.
- [45] S. J. Leigh, R. J. Bradley, C. P. Pursell, D. R. Billson, D. A. Hutchins, *PLoS One* **2012**, 7, e49365.
- [46] J. J. Adams, E. B. Duoss, T. F. Malkowski, M. J. Motala, B. Y. Ahn, R. G. Nuzzo, J. T. Bernhard, J. A. Lewis, *Adv. Mater.* **2011**, 23, 1335.
- [47] J. T. Muth, D. M. Vogt, R. L. Truby, Y. Mengüç, D. B. Kolesky, R. J. Wood, J. A. Lewis, *Adv. Mater.* **2014**, 26, 6307.
- [48] M. Gebler, A. J. S. Uiterkamp, C. Visser, *Energy Policy* **2014**, 74, 158.
- [49] H. N. Chia, B. M. Wu, *J. Biol. Eng.* **2015**, 9, 4.
- [50] E. Macdonald, R. Salas, D. Espalin, M. Perez, E. Aguilera, D. Muse, R. B. Wicker, *IEEE Access* **2014**, 2, 234.
- [51] Y. Xu, X. Wu, X. Guo, B. Kong, M. Zhang, X. Qian, S. Mi, W. Sun, *Sensors* **2017**, 17, 1166.
- [52] M. Vatani, Y. Lu, E. D. Engeberg, J. W. Choi, *Int. J. Precis. Eng. Manuf.* **2015**, 16, 1375.
- [53] A. Dijkshoorn, P. Werkman, M. Welleweerd, G. Wolterink, B. Eijking, J. Delamare, R. Sanders, G. J. M. Krijnen, *J. Sens. Sens. Syst.* **2018**, 7, 169.
- [54] M. Pawlaczyk, M. Lelonkiewicz, M. Wiczorowski, *Adv. Dermatol. Alergol.* **2013**, 30, 302.
- [55] P. Boonvisut, R. Jackson, M. C. Çavuşoğlu, presented at IEEE International Conference on Robotics and Automation, May 2012.
- [56] S. Eom, S. Lim, *Sensors* **2016**, 16, 1667.
- [57] S. Moscato, R. Bahr, T. Le, M. Pasian, M. Bozzi, L. Perregrini, M. M. Tentzeris, *IEEE Antennas Wireless Propag. Lett.* **2016**, 15, 1506.